applied sciences

Article

Effect of the Mid-Layer on the Diversion Length and Drainage Performance of a Three-Layer Cover with Capillary Barrier

Ayşenur Aslan Fidan * and Mehmet Muhit Berilgen *

Department of Civil Engineering, Davutpasa Campus, Yildiz Technical University, Istanbul 34230, Turkey
* Correspondence: aslana@yildiz.edu.tr (A.A.F.); mberilgen@yildiz.edu.tr (M.M.B.)

Abstract: The capillary barrier is a type of soil cover system commonly used in various geotechnical applications, such as limiting infiltration for slopes or landfills or providing cover for solid waste. It serves to prevent the movement of water through the soil layers by utilizing contrasting particle sizes. This paper focuses on investigating the effect of the granular layer on the performance of a three-layer cover with a capillary barrier, integrating the granular layer within clayey sand. The investigation involved one-dimensional infiltration tests utilizing four uniform granular soils with varying grain sizes. These tests were instrumental in calibrating soil water characteristic curves and hydraulic conductivity curves via back analysis. Subsequently, numerical analyses were conducted using a 15 m long model for each of the four distinct cover types. The results indicated that the fine gravel significantly improved the barrier performance beyond one-dimensional tests, owing to its high permeability and the influence of the slope. After the capillary barrier failure, the intermediate layers transitioned into efficient drainage layers, particularly in the gravel layer with the highest lateral drainage capacity. Clayey sand at the bottom delayed percolation, thereby supporting the conversion of the intermediate layer into an effective drainage component. Overall, the multi-layer system showed superior percolation performance compared to the clayey sand cover lacking a granular layer.

Keywords: three-layer cover system; capillary barrier; precipitation; diversion length; lateral drainage; water balance; unsaturated transient seepage analysis

Citation: Aslan Fidan, A.; Berilgen, M.M. Effect of the Mid-Layer on the Diversion Length and Drainage Performance of a Three-Layer Cover with Capillary Barrier. *Appl. Sci.* **2024**, *14*, 21. https://doi.org/10.3390/app14010021

Academic Editors: Ran An, Yixian Wang, Xianwei Zhang and Xinyu Liu

Received: 6 November 2023
Revised: 4 December 2023
Accepted: 14 December 2023
Published: 19 December 2023

1. Introduction

Capillary barriers, integral to preventing downward water movement through soil layers, consist of a fine-grained layer atop a coarser-grained soil [1–22]. Water infiltration into the fine-grained layer initially accumulates due to capillary forces, eventually leading to lateral movement once it reaches the interface between layers. Breakthrough occurs consistently at a set suction level, irrespective of the infiltration rate or finer layer characteristics. While some suggest the thickness of the coarse layer as negligible, others emphasize its direct impact on barrier effectiveness [23,24]. The capillary barrier effect is enhanced when the coarse layer contains soils exhibiting high uniformity and coarseness with low water entry suction [23,25]. Moreover, the characteristics of the coarse layer control the water storage capacity, infiltration rate, and system percolation [7].

The diversion length, a critical aspect in barrier design, profoundly affects water movement control. Smesrud and Selker [17] note substantial lateral diversion even with slight particle size contrast between fine and coarse materials. Methods proposed by Steenhuis et al. [26] and Ross [27] offer conservative estimations for diversion length calculation, while strategies like increasing the interface slope or incorporating heterogeneous finer layers with high horizontal permeability improve this length [7,10,14,28–32].

Effective capillary barriers necessitate the removal of infiltrated water from the fine layer through evaporation, evapotranspiration, and lateral diversion. Non-sloping configurations, particularly suitable for drier climates with high evaporation rates, demonstrate adequate performance with finer layers possessing high water retention capacity [13].

Researchers widely explore capillary barrier applications, notably in mitigating rainfall-induced slope failures and as covers for solid waste landfills [1–4,7–16,19–22,33–35]. These applications, validated through various testing methods, showcase the superiority of capillary barrier covers in terms of durability, cost-effectiveness, and performance over conventional low-permeability soil covers [7–16,19–22].

This study investigates the influence of various granular materials within the middle layer on the barrier effect, diversion length, lateral drainage, and system percolation of a three-layer cover featuring a capillary barrier (Figure 1). This three-layer configuration establishes a two-way capillary barrier, obstructing water movement caused by surface rainfall and rising water tables. However, this study does not consider the upward movement of water from the base, leaving this aspect for future exploration.

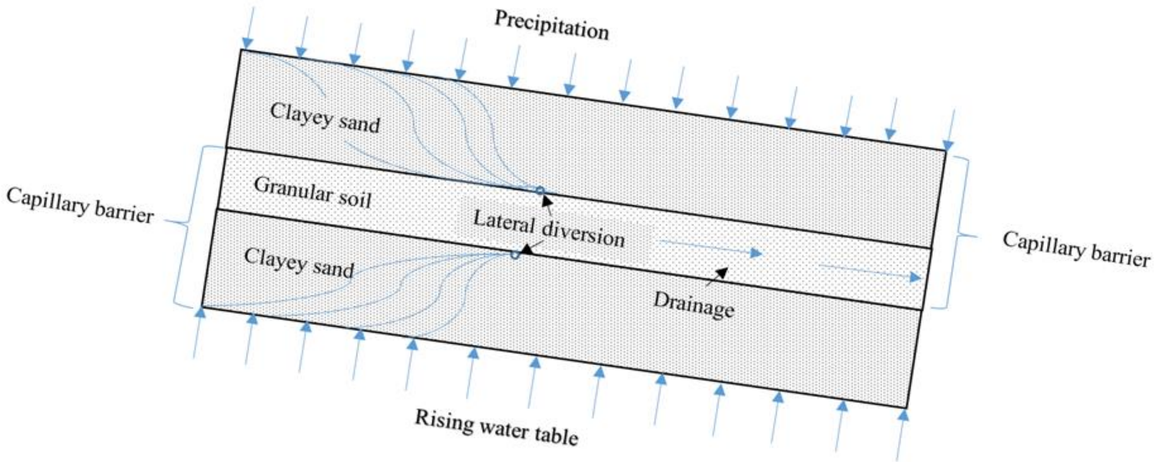

Figure 1. Design and mechanism of the three-layer cover with capillary barrier.

Previous studies extensively explored the impact of the coarse layer on the capillary barrier [23–25]. However, this study extends the investigation by incorporating a third layer beneath the barrier. Its objective is to examine the barrier effect and the subsequent effects of drainage and percolation within the three-layer cover after the barrier dissipates. Hence, experimental testing was conducted on the three-layer cover using soil column infiltration tests, employing four distinct mid-layer materials.

The experimental results were utilized for calibrating soil parameters, such as soil water characteristic curves and hydraulic conductivity curves, through a process of back analysis. Then, numerical analysis was used to compare the diversion length, lateral drainage, and percolation concerning the granular material used in the mid-layer with that of a 15 m model.

2. Materials

The properties of the soils used in the laboratory work are shown in Table 1. The granular materials used in this study were obtained commercially. These soils are poorly graded and have a uniform soil size of 95%, with a mean diameter ranging from 0.5 to 6 mm. The basic properties and soil water characteristic curves of the granular soils were obtained from previous research by Kesgin [36] in an experimental study on the drainage of sports fields. The clayey sand includes 26% fine content and is classified as clayey sand according to the Unified Soil Classification System (USCS). The plasticity index of the clayey sand soil is 8.5, and the clay friction (<0.002 mm) is about 10%, which affects the soil's hydraulic conductivity considerably.

Table 1. Properties of the soils.

Soil Type	Clayey Sand	Fine Sand	Medium Sand	Coarse Sand	Fine Gravel
Soil Classification (USCS)	SC	SP	SP	SP	GP
Gravel (%)	4	-	-	-	100 [1]
Sand (%)	70	100 [1]	100 [1]	100 [1]	-
Fine (%)	26	-	-	-	-
Mean diameter, D50 (mm)	0.45	0.5 [1]	1.0 [1]	1.19 [1]	6.0 [1]
Coefficient of uniformity, Cu	440	1.47 [1]	1.57 [1]	1.90 [1]	1.40 [1]
Coefficient of curvature, Cc	5.2	1.05 [1]	1.13 [1]	1.54 [1]	0.96 [1]
Liquid limit, LL (%)	28.5	-	-	-	-
Plastic limit, PL (%)	20	-	-	-	-
Specific gravity, Gs	2.7	2.65 [1]	2.72 [1]	2.66 [1]	2.65 [1]
Saturated permeability, k_{sat} (m/s)	2.54×10^{-7}	8.27×10^{-4} [1]	2.60×10^{-3} [1]	4.9×10^{-3} [1]	1.07×10^{-2} [1]

[1] Kesgin [36].

The soil water characteristic curve of the clayey sand was determined by conducting a pressure plate test following ASTM (D6836-16) guidelines at various void ratios. The data obtained from these tests, including volumetric water content and matric suction, were then analyzed and fitted using van Genuchten's equation [37] (Figure 2a) to obtain comprehensive curves across the entire range.

$$\theta(\Psi) = \theta_r + \frac{\theta_s - \theta_r}{[1 + (\alpha\Psi)^n]^m} \quad (1)$$

where $\theta(\psi)$ is the volumetric water content at a given matric potential ψ, θ_s is the volumetric water content at saturation, θ_r is the residual volumetric water content, and α, n, and m are the van Genuchten fitting parameters. The curve fitting parameters obtained are presented in Table 2. A falling head permeability test, in accordance with ASTM (D5856-15) standards, was conducted on the clayey sand to determine the permeability coefficient.

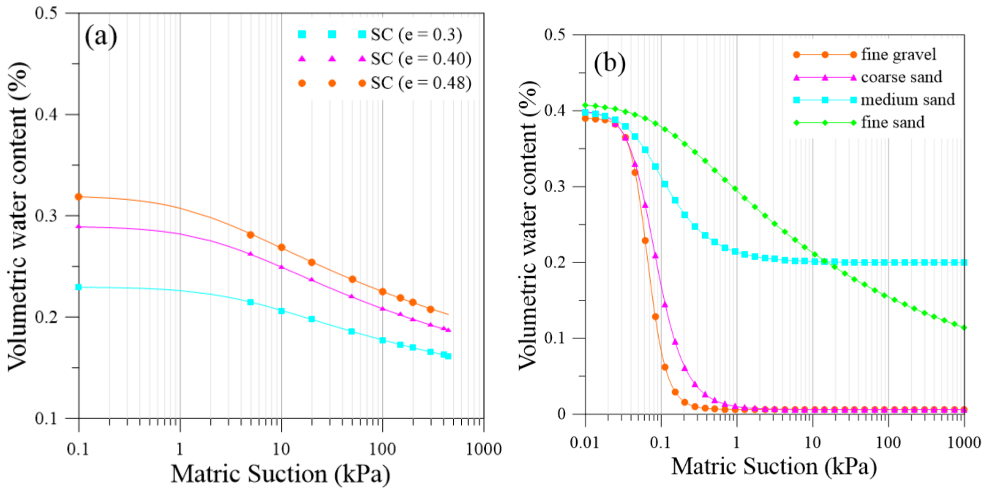

Figure 2. SWCCs of soils, (**a**) clayey sand and (**b**) granular soils [36].

Table 2. van Genuchten parameters of the soil water characteristic curves.

Soil Type	θ_s	θ_r	α (kPa)	n
SC (e = 0.48)	0.32	0.1	1.4407	1.1341
SC (e = 0.40)	0.29	0.1	2.3403	1.1482
SC (e = 0.30)	0.23	0.1	3.4807	1.1523
Fine gravel	0.39 [1]	0.006 [1]	0.0606 [1]	4.0 [1]
Coarse sand	0.4 [1]	0.006 [1]	0.0662 [1]	2.7 [1]
Medium sand	0.4 [1]	0.02 [1]	0.06896 [1]	1.99 [1]
Fine sand	0.41 [1]	0.023 [1]	0.11627 [1]	1.16 [1]

[1] Kesgin [36].

3. Test Setup

The three-layered soil system constructed in the cylindrical container is shown in Figure 3. The experimental setup contained three main components, which were (a) the soil column compacted in a cylindrical transparent Plexiglas tube with a diameter of 16 cm, (b) the precipitation simulator, a peristaltic pump to achieve a constant precipitation rate, and (c) the measuring instruments: TDR, tipping bucket, data logger, and computer.

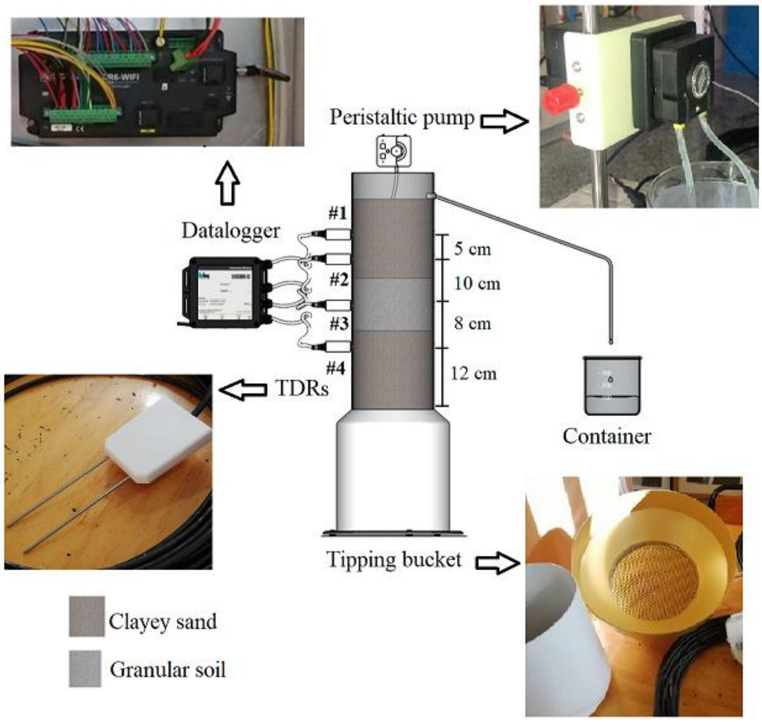

Figure 3. Schematic view of the test setup.

The top and bottom soils were layered and compacted during the soil column tests to attain the specified bulk density and water content, as illustrated in Table 3. These values were on the drier side of the optimum water content. The materials used in the middle layer, comprising fine sand, medium sand, coarse sand, and fine gravel, were vibrated with a hammer to achieve the targeted density specified in Table 3. The soil column's top and bottom layers were 15 cm in height, while the middle layer was 10 cm in height. Precipitation was applied to the soil surface at a 1 mL/min rate using a Longer Pump model BQ50-1J peristaltic pump. Surface runoff was directed through a pipe placed in a hole drilled in the Plexiglas. The pipe was positioned at ground level to prevent ponding. Several holes were drilled along the side walls of the Plexiglas tube to install the instruments in the soil column. Four model CS655 (Campbell Scientific) TDRs (Time Domain Reflectometers) were installed at different depths—12 cm, 20 cm, 30 cm, and

35 cm—to monitor moisture content. Two were placed in the top layer, one in the middle, and one in the bottom. TDR sensors assess the dielectric conductivity of the environment rather than at a specific point, requiring accurate positioning to avoid interactions between sensors. The TDR configuration has been optimized to overcome this problem. For the 1D infiltration tests, infiltration was applied to the soil surface at a 1 mL/min rate using the Longer Pump BQ50-1J peristaltic pump. The soil column was positioned on the tipping bucket (Texas Electronics Inc. Dallas, TX, USA TR-525M), which included a perforated metal plate resembling a grid. This setup allowed water drainage and measured percolated water using tipping buckets (Figure 3).

Table 3. The initial condition of the soil layers for each test.

Test Name	Bulk Density (gr/cm^3)			Initial Water Content (%)			Precipitation Rate (mm/h)
	Top	Middle	Bottom	Top	Middle	Bottom	
SC-3L-FG	2	1.5	2	8	-	8	3
SC-3L-CS	2	1.5	2	8	-	8	3
SC-3L-MS	2	1.5	2	8	-	8	3
SC-3L-FS	2	1.5	2	8	-	8	3

4. Results and Discussion

The changes in the volumetric water content over time were examined across four separate soil columns during the infiltration experiments. In each test, the increase in the volumetric water content in the top layer began approximately 1.5 h after the start for TDR1, situated 5 cm from the soil surface, and after 5 h for TDR2, positioned 10 cm below the soil surface. Interestingly, despite the middle layers having higher permeability, delays in water movement through these layers were observed for varying durations (Figure 4).

In the fine sand test (SC-3L-FS), an increase in the volumetric water content of TDR-3, positioned below the interface, was noted after approximately 54.5 h. The water content in the fine sand displayed a time-dependent and gradual increase, while a similar rise in the water content of the bottom layer was observed after roughly 114 h. A rise in the volumetric water content of approximately 5% was recorded in the middle layer, whereas 7% was measured in the lower layer. Throughout the 500 h test, no percolation was observed, and the column did not reach a steady-state condition.

During the medium sand test (SC-3L-MS), the volumetric water content of TDR-3, positioned below the interface, began to slightly increase after approximately 92.5 h. This observation indicates that the medium sand, characterized by higher saturated conductivity than fine sand, retained water at the interface for an extended duration. While the water content increased by only 3% in the middle layer, the bottom layer became wetted slightly faster and retained more water than the middle layer. Additionally, despite the water requiring more time to infiltrate the middle layer with medium sand present, the volumetric water content in the bottom layer increased earlier (approximately at 102 h) compared to the test with fine sand (SC-3L-FS). Percolation did not occur during the test, and the change in volumetric water content did not stabilize.

In the SC-3L-CS test, where coarse sand was placed in the middle of the soil column, no initial change in the volumetric water content was observed in TDR-3. However, a marginal increase in the volumetric water content in the third layer was noted after 68 h. Unfortunately, the test was terminated at 350 h due to issues with the peristaltic pump, and no percolation was observed.

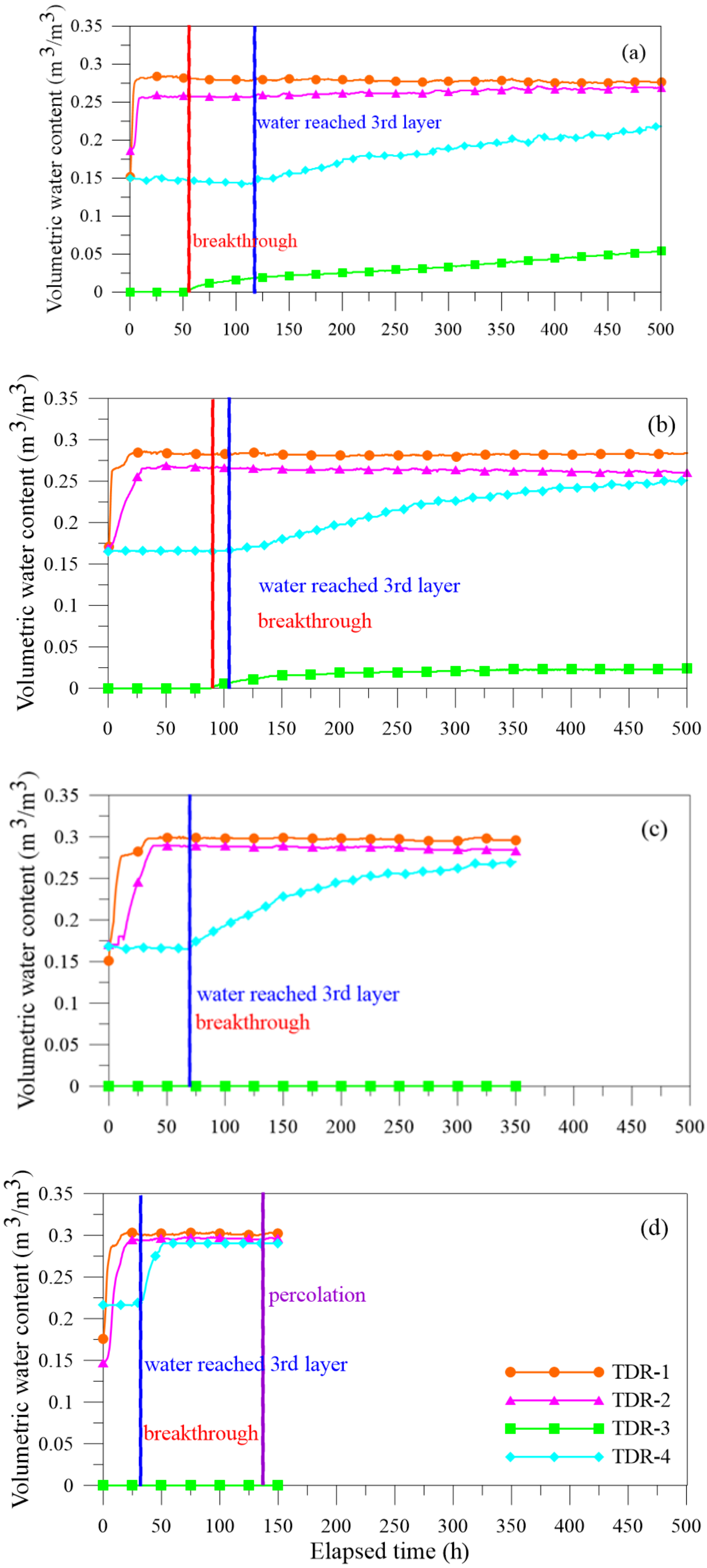

Figure 4. Volumetric water content variation with time and depth for soil column infiltration tests. (**a**) SC-3L-FS, (**b**) SC-3L-MS, (**c**) SC-3L-CS, and (**d**) SC-3L-FG.

In the SC-3L-FG test involving fine gravel in the middle layer, a notable increase in the volumetric water content in the third layer became evident at the 26th h, indicating a breakthrough. Similar to the experiment with coarse sand, there were no significant changes in TDR-3 readings. Once the volumetric water contents reached equilibrium, percolation commenced at the 135th h.

The measurement of volumetric water content within both the coarse sand and fine gravel columns in the coarse-grained layer could not detect the increase in volumetric water content during the infiltration process. This occurrence might be explained by the presence of preferential flow within the coarse-grained layer, as highlighted in previous studies [23,32,38]. Preferential water flow refers to a scenario where a majority (i.e., 70–85%) of water movement in the unsaturated zone follows specific pathways, bypassing the surrounding soil matrix with limited resistance [39–41].

This preferential flow, often resembling fingering, becomes notably visible when transitioning from a fine-grained layer to an underlying coarse-grained layer, as observed in systems like the capillary barrier [42]. This phenomenon tends to occur when the coefficient of permeability at the water entry value of the coarse-grained layer exceeds the infiltration flux from the fine-grained layer [32,43].

However, the fingering flow within the coarse-grained layer did not significantly impact the fundamental outcomes of the experiments concerning the water storage of the tests. This is attributed to the fact that similar physical characteristics governed both fingering and breakthrough within the coarse-grained layer, specifically the water entry value of the underlying coarse-grained soil [32,44]. Additionally, the water content increased by 5% in fine sand and 3% in medium sand throughout the experiment. However, the water retained in the soil against gravitational forces during precipitation or infiltration depends on the soil's water-holding capacity, which tends to be relatively low in coarse-grained soils [45].

4.1. Breakthrough Time

The evaluation of water entry into the middle layer during experiments, represented by breakthrough time, aimed to consider the increase in volumetric water content in the coarse layer. However, as previously mentioned, this increase could not be detected in the coarse sand and fine gravel. Contrastingly, in Figure 5, it is observable that as the grain size increases in the middle layer, the breakthrough time and the duration of the volumetric water content increase in the third layer converge. Consequently, the breakthrough time for these layers is considered the moment when the volumetric water content of the third layer starts to increase. The most prolonged barrier performance was observed when the medium sand was used in the middle layer of the cover (Figure 5).

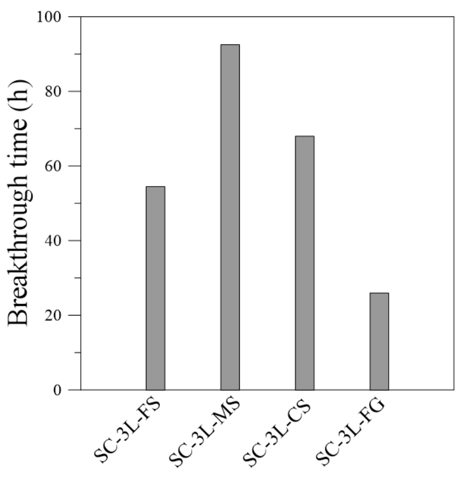

Figure 5. Breakthrough time for each soil column infiltration test.

The coarser materials generally exhibit steeper soil water characteristic curves (SWCCs) due to their lower water retention capacity. Therefore, even small changes in the volumetric water content may result in significant shifts in matric suction. In soil column tests, as grain size increased in the middle layer, more water was retained near the interface (Figure 4). This condition could cause a faster and more substantial change in water potential at the interface, leading to a faster breakthrough in the fine gravel test. This finding is consistent with the results of [25]. It indicates that using medium sand in the test, rather than gravel in the coarser layer, is more effective in maintaining the barrier effect.

4.2. Ultimate Volumetric Water Content and Water Storage

The changes in the volumetric water content allowed the determination of the water storage in the soil layers [3,25,32]. Observing the water storage of the cover over time during the tests reveals a correlation with the coarseness of the middle layer. Intriguingly, although the earliest breakthrough occurred in the section using fine gravel, the highest water storage was noted when gravel was employed in the middle layer, even before the breakthrough (Figure 6). Across all covers, a sharp increase in water storage was observed at the beginning of infiltration in the first layer. Subsequently, this increasing trend diminished for varying durations before rising again post-breakthrough, where the third layer began to store water.

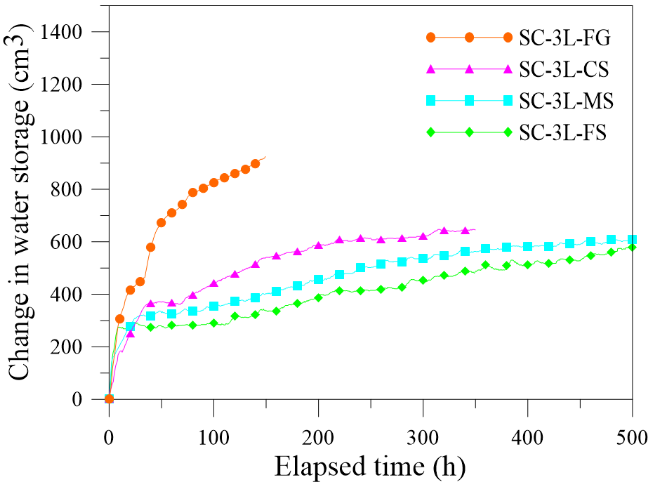

Figure 6. The change in water storage of soil columns during infiltration tests.

In addition, Figure 7 demonstrates an increment in the final volumetric water content of the top layer as the gradation of the middle layer increases. The middle layer's influence on the upper layer's volumetric water content is particularly noticeable near the interface. A breakthrough occurs when the water potential at the interface reaches the water entry value of the coarse layer. The coarser soil generally has a lower water entry value [23–25]. Therefore, water infiltration into coarser-grained soils (e.g., fine gravel) occurred after the upper layer reached a higher saturation level than in other experiments.

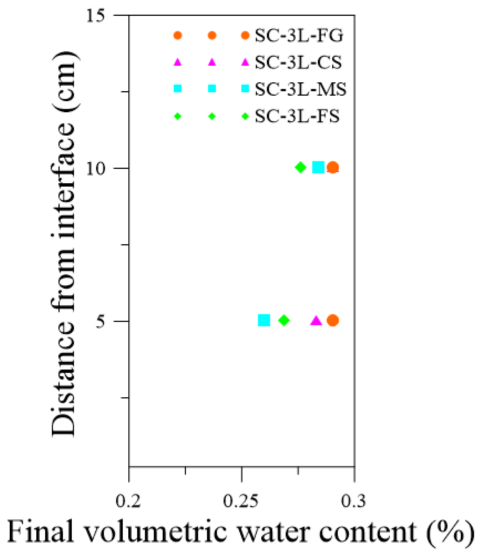

Figure 7. Final volumetric water content of the top layer.

4.3. Water Balance

The water balance was precisely assessed during the experiments, considering the measurements taken throughout the tests. Simultaneously, surface flow was measured at specific intervals during the experiment. Additionally, percolation was carefully measured using a tipping bucket, and measurements were recorded by the data logger at regular intervals. These comprehensive measurements enabled a thorough evaluation of the water balance in the soil column tests.

The water balance graph of the SC-3L-FG test in which percolation occurred, shown in Figure 8, reveals several significant findings. In the other tests, only water storage occurred, and the time-dependent storage changes across all experiments given in Figure 8 demonstrate that out of the total rainfall received, only 10% was retained within the soil layers, a mere 0.2% infiltrated as percolation, and the majority transformed into surface runoff. This outcome indicates that the amount of rainfall applied exceeded the saturated permeability of the upper soil layer, mainly due to its low permeability. Consequently, a substantial portion of the rainfall became surface runoff throughout the experiment.

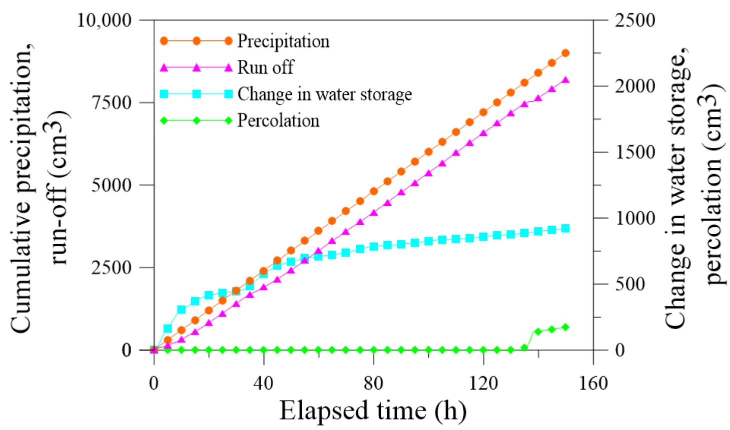

Figure 8. The water balance of the cover with fine gravel.

The experiments revealed challenges in sensitively measuring assessing soil infiltration due to the manual measurement of very high runoff and the need to account for evaporation over extended experiment durations. To address these issues and evaluate the infiltration rate during the tests, a modified parameter known as "net infiltration" was introduced. Net infiltration accounts for the effective amount of water infiltrating the soil, considering factors such as evaporation and measurement errors. Consequently, the net infiltration value was calculated as the sum of water storage and percolation. This adjustment aimed to provide a more accurate representation of the soil column test by addressing these factors. The infiltration rates of the tests are shown in Figure 9.

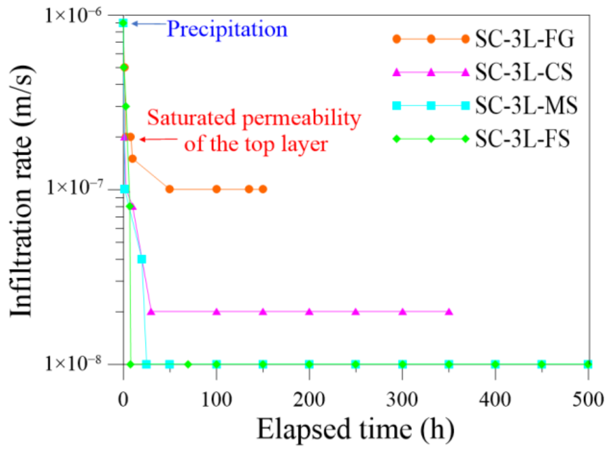

Figure 9. Infiltration rate variation with time for all tests.

Based on the data shown in Figure 9, the infiltration rates in all tests, except for the gravel case, are significantly lower than the saturated hydraulic conductivity of the top layer. This observation suggests that the granular layers remain unsaturated after the breakthrough, which may limit the overall infiltration into the system. In addition, the breakthrough may have occurred in only a portion of the cross-section. This leads to the assumption that the progress of the water to the third layer is restricted for some time after the breakthrough. In the experimental study by Qian et al. [24], visualizations with colored liquid show that the barrier is initially broken at one point along the cross-section, and over time, the barrier effect disappears along the entire interface. Except for the experiment with gravel in the middle layer, no steady-state flow occurred after the breakthrough in the other sections. When comparing the materials used in the middle layer, it is apparent that the lowest infiltration rate was observed in the cases of fine and medium sand. In contrast, the highest infiltration rate was observed in the experiment employing gravel as the middle layer material.

4.4. Numerical Study on the Performance of Three-Layer Covers with Capillary Barrier

Previous tests emphasized the mid-layer's impact on the capillary barrier effect within a three-layer cover. However, due to constraints related to test equipment and geometric dimensions, the physical tests could not assess the cover's performance at the engineering scale. Numerical modeling should be approached not as a predictive tool but as a means to gain deeper insights into the behaviors of complex systems across various scenarios [46]. A 15 m long cover was numerically investigated to address this, enabling comparisons of diversion length, lateral drainage, and percolation across various mid-layers. Numerical analyses were conducted using the SEEP/w (GEOSTUDIO 2023.1) software based on the finite element method.

Unsaturated soil exhibits hysteric behavior, with significant differences observed in the drying and wetting soil water characteristic curves (SWCCs) [47–50]. These curves also experience changes when subjected to repeated wetting and drying processes. Using appropriate soil properties, such as SWCCs, in numerical analyses is crucial to modeling soil behavior accurately under unsaturated conditions [38–50]. Back analyses were performed to calibrate the soil water characteristics and hydraulic conductivity curves based on the results of the 1D infiltration tests.

4.4.1. Back Analysis of the Physical Model Test

The model's geometry and boundary conditions were based on the laboratory model employed. Flux boundary conditions were used to apply precipitation on the soil surface by using a net infiltration rate [2,3,18,51]. Zero-flux boundary conditions were assigned to the left and right sides of the soil column to create an impermeable condition [3,52]. A unit gradient boundary condition was imposed at the bottom of the soil column to facilitate water drainage [3]. The model's geometry and boundary conditions for the soil columns can be observed in Figure 10.

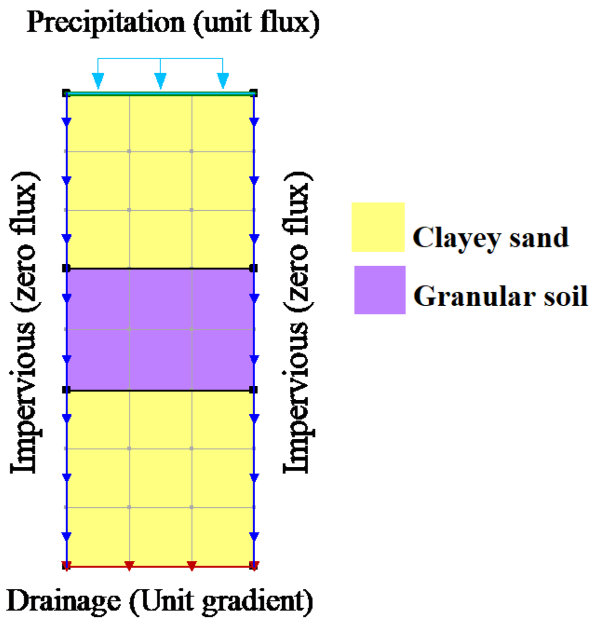

Figure 10. Model geometry and boundary conditions.

The calibrated SWCCs, representing the wetting properties of the soils, are presented in Figure 11. Experimentally measuring hydraulic conductivity curves can be a time-consuming and expensive effort. Therefore, methods for estimating hydraulic conductivity based on SWCCs and the saturated permeability of the soil have provided reasonable results in both scientific research and practical site applications [53]. In this study, the van Genuchten–Muallem [37,54] method was selected to define the hydraulic conductivity of the soils in the numerical model.

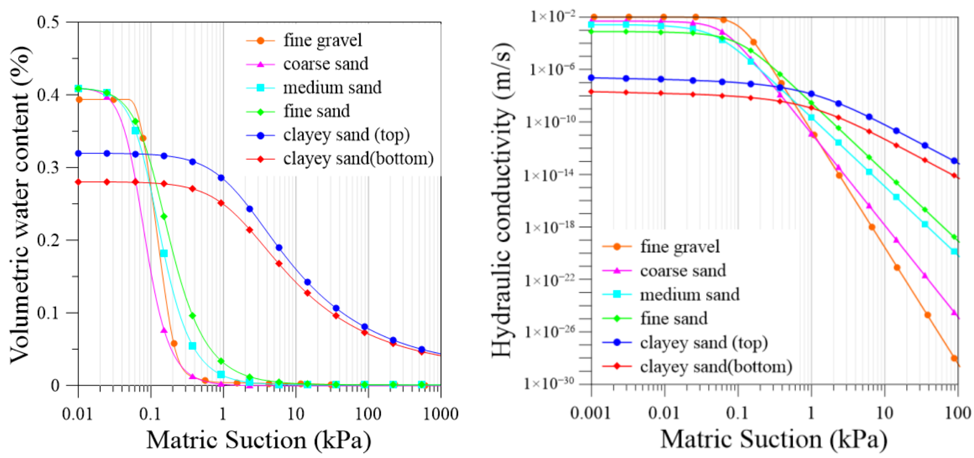

Figure 11. Calibrated SWCCs and HCFs of the soils.

Calibrated SWCC data were utilized to derive the curves, as illustrated in Figure 11. Moreover, the permeability of the bottom layer used in the analyses was reduced to 4×10^{-8} m/s, below the measured value. This adjustment accounted for the double compaction applied to the bottom layer. This assumption was based on the percolation observed during the gravel test.

The numerical analysis illustrates the variation in volumetric water content across the entire depth of the soil column. Figure 12 represents this variation over time, derived through back analysis for each test. Additionally, the experimental test results are integrated into Figure 10 for comparison.

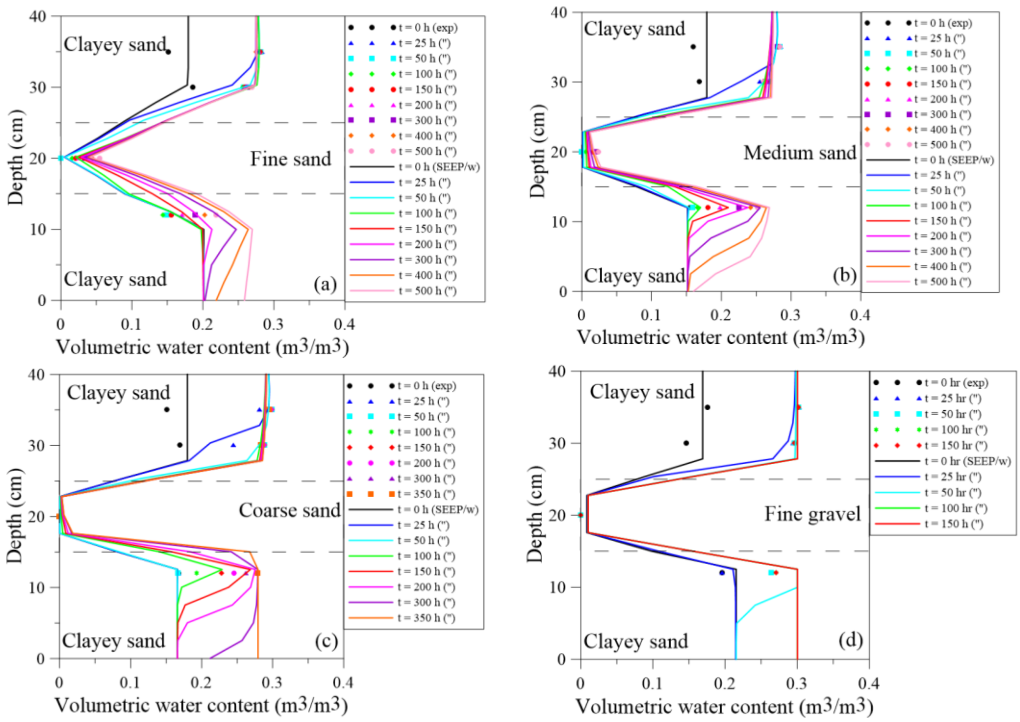

Figure 12. Volumetric water content variation with depth and time obtained from back analysis, (**a**) fine sand, (**b**) medium sand, (**c**) coarse sand, and (**d**) fine gravel.

Given the calibration of soil water characteristic curves (SWCCs) and Hydraulic Conductivity Functions (HCFs) for each soil layer, the changes in the volumetric water content obtained from the numerical analysis align remarkably well with the experimental results. Breakthrough occurs almost simultaneously with the laboratory tests. The trend in the volumetric water content changes calculated from the numerical analysis mirrors that observed in the laboratory test results.

While experimental measurements offer limited data points along the column, their strategic placement in areas demonstrating significant changes ensures an accurate representation of the soil column. Notably, the findings from the numerical study correspond with the observed low water retention capacities in the experimental section.

4.4.2. Comparison of the Diversion Length, Lateral Drainage, and Percolation of the Covers

This section focuses on the diversion length, lateral drainage, and percolation within the three-layer cover with a capillary barrier. A model, 15 m in length, was employed to observe its lateral diversion capabilities. Layer thicknesses remained consistent in the experimental setup. The model's total height is 70 cm along the long edge and 30 cm along the short edge, introducing a 3% slope to the capillary barrier. This slope adjustment allows for natural gravitational water movement. The analyses utilized previously validated relationships. The lateral diversion length was computed using Aubertin et al.'s [51] proposed method. Breakthrough points, identified where pore pressure dropped below the water entry value of the coarser layer at each time interval, determined the lateral diversion length in the model (see Figure 13).

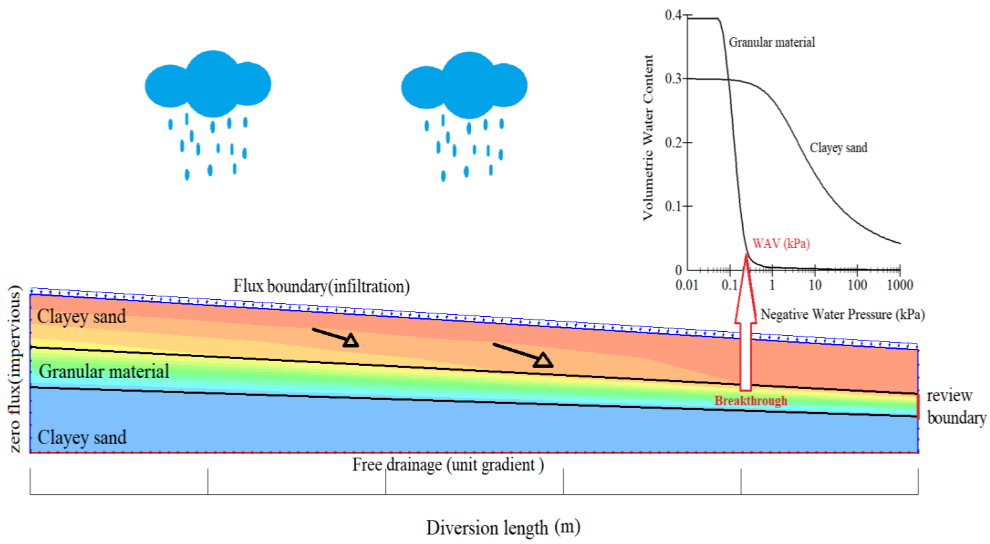

Figure 13. Schematic view of the Aubertin method (2009) [51].

The model's boundary conditions closely resemble those used in the 1D experiments, with one notable difference: a review boundary condition was applied to the granular layer at the bottom edge. This condition aligns with the approach outlined in Zhan et al.'s study [33] (Figure 13). In the 1D tests, most rainfall primarily resulted in surface runoff. The numerical calculations adopted relatively low infiltration rates of 1 mm/day, 3.5 mm/day, and 8.6 mm/day.

The numerical models account for changes in diversion length over time, alterations in the lateral flow of drained water within the granular layer over time, and the progression of percolation.

A notable distinction emerged in the analysis of four sections under varying rainfall conditions (Figure 12). Unlike the one-dimensional experiments, numerical analyses revealed that fine gravel, coarse sand, and medium sand showed remarkably similar behavior over time. In one-dimensional scenarios, water retention at the interface without horizontal drainage eventually led to barrier failure. However, water mobility along the interface prolonged the barrier effect in two-dimensional configurations and inclined barriers. Lateral diversion predominantly occurs at the fine/coarse interface, where hydraulic conductivity tends to be highest [10]. The numerical analysis results concerning lateral diversion are attributed to the high permeability of the gravel material and coarse sand, which facilitates faster water movement at the interface and increases the barrier effect. Conversely, fine sand has a reduced performance due to its high water entry value and low permeability. Moreover, increased rainfall reduced diversion lengths in each section, as noted by [51], subsequently minimizing discrepancies between the sections. During the 8.6 mm/day infiltration, the increased infiltration rate may exceed the lateral drainage capacity. At this point, the impact of the hydraulic conductivity of the middle layer on the diversion becomes less apparent (Figure 14).

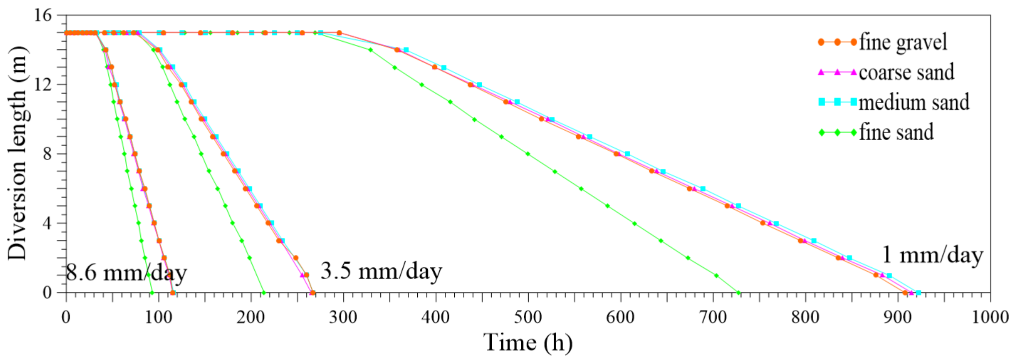

Figure 14. Change in diversion length over time with varying infiltration rate.

The influence of the middle layer on lateral drainage was investigated during a relatively high rainfall event with an intensity of 8.6 mm/day (Figure 15). As expected, fine gravel showed the most effective lateral drainage performance, resulting in the highest lateral flow. Conversely, fine sand showed the poorest performance, with minimal lateral drainage due to its low permeability. For all soil types, lateral drainage started almost immediately after the capillary barrier effect completely disappeared, reached a maximum value, and remained stable.

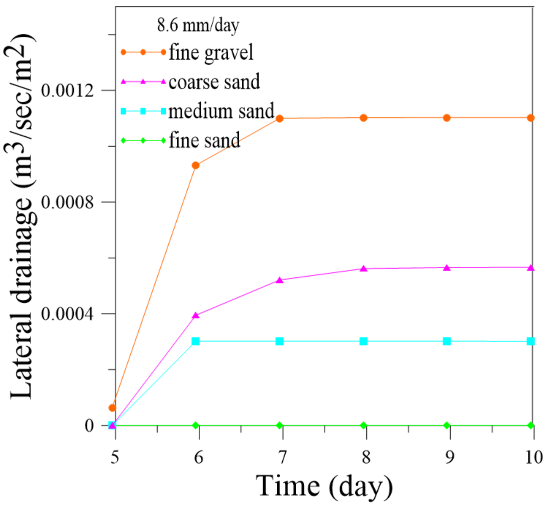

Figure 15. Variation in lateral drainage of the middle layers over time at an infiltration rate of 8.6 mm/day.

Comparisons of percolation in multi-layer covers at an infiltration rate of 3.5 mm/day were conducted to evaluate the influence of the middle layer (Figure 16). Additionally, numerical analysis assessed percolation within the clayey sand section (without any granular layer). Time-dependent variations in deep percolation across distances revealed interesting insights.

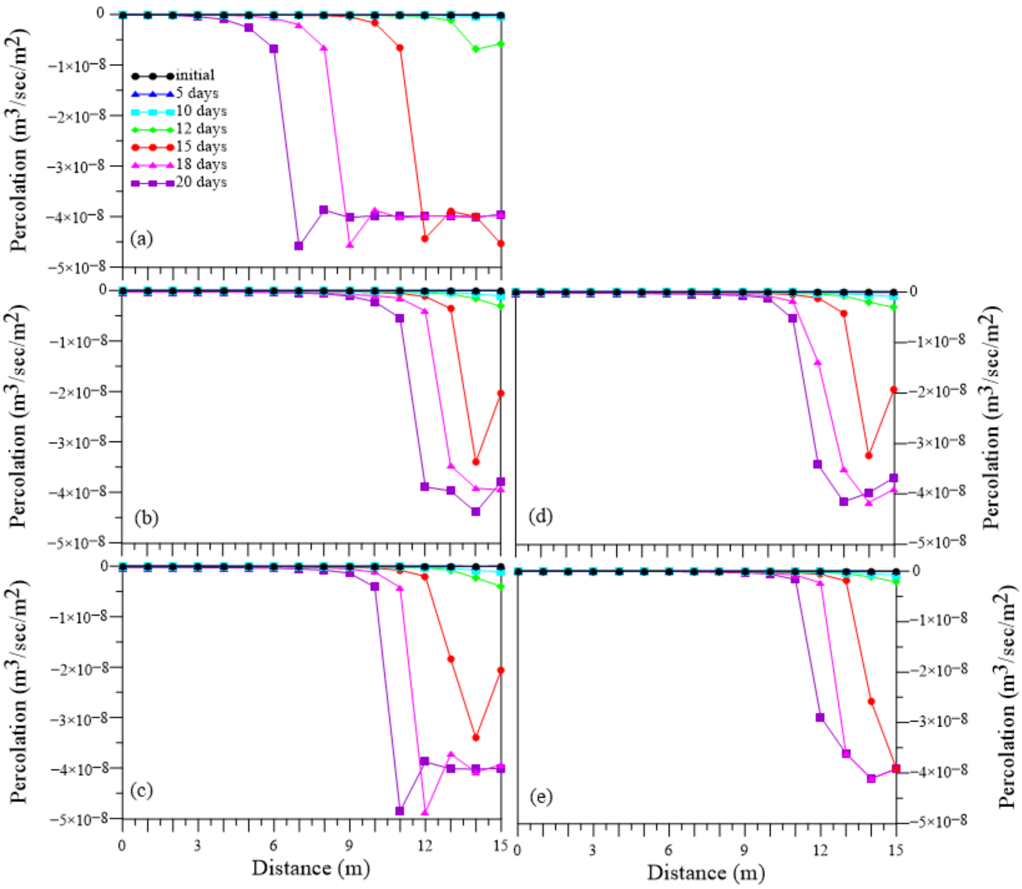

Figure 16. Percolation variation over distance and time, (**a**) clayey sand, (**b**) fine gravel, (**c**) coarse sand, (**d**) medium sand, and (**e**) fine sand.

Unexpectedly, when examining the time-dependent changes in percolation across all models, the typically less permeable clayey sand model showed the poorest performance. Percolation occurred along half of the cover in this area, mainly in the lower elevation region. However, percolation was only observed across a third of the cover in sections with a granular layer. This difference could be attributed to water diversion by the barrier effect and subsequent lateral water drainage through the granular layer after the complete dissipation of the barrier (approximately 12 days).

Percolation was observed in all sections featuring granular material in the middle layer only after the capillary barrier effect had completely dissipated. Despite all models with a granular mid-layer performing equally or even better than the clayey sand model, those with medium sand exhibited the best performance. Notably, the quantity of percolating water in all models aligned with the overall system's saturated permeability and remained highly consistent across the range.

5. Conclusions

This study includes an in-depth investigation of a multi-layer cover system utilizing four different granular materials within the intermediate layer, employing a combination of experimental results and numerical analyses.

During the experimental phase, the most notable success in terms of the duration of the barrier effect was achieved when using medium sand in the middle layer. However, the highest capacity for water retention within the multi-layer cover system during the capillary barrier was reached by fine gravel.

Based on the experimental findings, this study conducted back analyses to calibrate the soil water characteristic curves (SWCCs) and Hydraulic Conductivity Functions (HCFs). In subsequent two-dimensional analyses, mainly when accounting for lateral diversion length, the barrier performance of the fine gravel exhibited a marked improvement compared to one-dimensional calculations. This enhancement can be attributed to the rapid movement of water at the interface due to the high permeability of gravel, an effect further enhanced by the slope.

Furthermore, following the failure of the capillary barrier in the upper section, it was observed that the intermediate layers were transformed into drainage layers. Notably, the gravel layer demonstrated the highest lateral drainage capacity among them. Additionally, a clayey sand layer at the base of the multi-layer system resulted in delayed percolation. It facilitated the conversion of the intermediate layer into an efficient drainage layer. In addition, the percolation performance of the multi-layer system is superior to that of the clayey sand cover without a granular layer.

6. Limitations and Considerations

This study provides superficial results on the behavior of a three-layer cover with different middle layers. However, the experimental study did not consider the influence of factors such as different rainfall intensities, initial conditions, layer thicknesses, and slopes. Similarly, the numerical analysis did not consider layer thickness, repeated rainfall effects, evaporation or wet–dry cycles, capillary barrier recovery, freeze–thaw effects on the barrier, or desiccation cracking. In addition, this study did not consider the behavior of the barrier during bottom-up water movement. These are critical issues that should be addressed in future studies to evaluate the performance of the three-layer barrier liner thoroughly.

Author Contributions: Conceptualization, A.A.F. and M.M.B.; methodology, A.A.F. and M.M.B.; software, A.A.F.; validation, A.A.F.; formal analysis, A.A.F.; investigation, A.A.F.; resources, A.A.F.; data curation, A.A.F.; writing—original draft preparation, A.A.F.; writing—review and editing, A.A.F. and M.M.B.; visualization, A.A.F.; supervision, M.M.B. All authors have read and agreed to the published version of the manuscript.

Funding: This research is supported by research grant 217M561 'Solution Proposals for the Preservation and Rehabilitation of Traditional Flat Earthen Roofs of Kemaliye Houses' from the Scientific and Technological Research Council of Turkey (TUBITAK).

Institutional Review Board Statement: Not applicable.

Informed Consent Statement: Not applicable.

Data Availability Statement: All data are included in this article.

Acknowledgments: The authors would like to thank master science student Firat Sargin for his support during the laboratory tests submitted in this study.

Conflicts of Interest: The authors declare no conflict of interest.

References

1. Rahardjo, H.; Santoso, V.A.; Leong, E.C.; Ng, Y.S.; Hua, C.J. Performance of an instrumented slope covered by a capillary barrier system. *J. Geotech. Geoenviron. Eng.* **2012**, *138*, 481–490. [CrossRef]
2. Rahardjo, H.; Krisnanto, S.; Leong, E.C. Effectiveness of capillary barrier and vegetative slope covers in maintaining soil suction. *Soils Rocks* **2016**, *39*, 51–69. [CrossRef]
3. Tami, D.; Rahardjo, H.; Leong, E.-C.; Fredlund, D.G. Design and laboratory verification of a physical model of sloping capillary barrier. *Can. Geotech. J.* **2004**, *41*, 814–830. [CrossRef]
4. Tami, D.; Rahardjo, H.; Leong, E.-C.; Fredlund, D.G. A Physical Model for Sloping Capillary Barriers. *Geotech. Test. J.* **2004**, *27*, 173–183.
5. Mancarella, D.; Simeone, V. Capillary barrier effects in unsaturated layered soils, with special reference to the pyroclastic veneer of the Pizzo d'Alvano, Campania, Italy. *Bull. Eng. Geol. Environ.* **2012**, *71*, 791–801. [CrossRef]
6. Tang, J.; Taro, U.; Huang, D.; Xie, J.; Tao, S. Physical model experiments on water infiltration and failure modes in multi-layered slopes under heavy rainfall. *Appl. Sci.* **2020**, *10*, 3458. [CrossRef]
7. Stormont, J.C. The effectiveness of two capillary barriers on a 10% slope. *Geotech. Geol. Eng.* **1996**, *14*, 243–267. [CrossRef]
8. Malusis, M.A.; Benson, C.H. Lysimeters versus Water-Content Sensors for Performance Monitoring of Alternative Earthen Final Covers. In *Unsaturated Soils 2006*; ASCE: New York, NY, USA, 2006; Volume 147, pp. 741–752.

9. Williams, L.O.; Hoyt, D.L.; Dwyer, S.F.; Hargreaves, G.A.; Zornberg, J.G. Design Criteria and Construction of a Capillary Barrier Cover System: The Rocky Mountain Arsenal Experience. In Proceedings of the GeoFrontiers 2011 Conference, Geo-Institute of ASCE, Dallas, TX, USA, 13–16 March 2011.
10. Morris, C.E.; Stormont, J.C. Evaluation of numerical simulations of capillary barrier field tests. *Geotech. Geol. Eng.* **1998**, *16*, 201–213. [CrossRef]
11. Khire, M.V.; Benson, C.H.; Bosscher, P.J. Field data from a capillary barrier and model predictions with UNSAT-H. *J. Geotech. Geoenviron. Eng.* **1999**, *125*, 518–527. [CrossRef]
12. Benson, C.H.; Albright, W.H.; Roesler, A.C.; Abichou, T. Evaluation of Final Cover Performance: Field Data from the Alternative Cover Assesment Program (ACAP). In Proceedings of the WM '02 Conference, Tucson, AZ, USA, 24–28 February 2002.
13. Abdolahzadeh, A.M.; Lacroix Vachon, B.; Cabral, A.R. Assessment of the design of an experimental cover with capillary barrier effect using 4 years of Field Data. *Geotech. Geol. Eng.* **2011**, *29*, 783–802. [CrossRef]
14. Morris, C.E.; Stormont, J.C. Capillary barriers and subtitle D covers: Estimating equivalency. *J. Environ. Eng.* **1997**, *123*, 3–10. [CrossRef]
15. Morris, C.E.; Stormont, J.C. Parametric study of unsaturated drainage layers in a capillary barrier. *J. Geotech. Geoenviron. Eng.* **1999**, *125*, 1057–1065. [CrossRef]
16. Khire, M.V.; Benson, C.H.; Bosscher, P.J. Capillary barriers: Design variables and water balance. *J. Geotech. Geoenviron. Eng.* **2000**, *126*, 695–708. [CrossRef]
17. Smesrud, J.K.; Selker, J.S. Effect of Soil-Particle Size Contrast on Capillary Barrier Performance. *J. Geotech. Geoenviron. Eng.* **2001**, *127*, 885–888. [CrossRef]
18. Li, J.H.; Du, L.; Chen, R.; Zhang, L.M. Numerical investigation of the performance of covers with capillary barrier effects in South China. *Comput. Geotech.* **2013**, *48*, 304–315. [CrossRef]
19. Ogorzalek, A.S.; Bohnhoff, G.L.; Shackelford, C.D.; Benson, C.H.; Apiwantragoon, P. Comparison of Field Data and Water-Balance Predictions for a Capillary Barrier Cover. *J. Geotech. Geoenviron. Eng.* **2008**, *134*, 470–486. [CrossRef]
20. Fala, O.; Molson, J.; Aubertin, M.; Bussière, B. Numerical Modelling of Flow and Capillary Barrier Effects in Unsaturated Waste Rock Piles. *Mine Water Environ.* **2005**, *24*, 172–185. [CrossRef]
21. Shackelford, C.D.; Benson, C.H. Selected Factors Affecting Water-Balance Predictions for Alternative Covers Using Unsaturated Flow Models. In *GeoCongress 2006: Geotechnical Engineering in the Information Technology Age*; ASCE: New York, NY, USA, 2006.
22. Aubertin, M.; Cifuentes, E.; Martin, V.; Apithy, S.; Bussiere, B.; Molson, J.; Chapuis, R.P.; Maqsoud, A. An Investigation of Factors that Influence the Water Diversion Capacity of Inclined Covers with Capillary Barrier Effects. In *Unsaturated Soils 2006*; ASCE: New York, NY, USA, 2006. [CrossRef]
23. Stormont, J.C.; Anderson, C.E. Capillary Barrier Effect from Underlying Coarser Soil Layer. *Geotech. Geoenviron. Eng.* **1999**, *125*, 641–648. [CrossRef]
24. Qian, T.; Huo, L.; Zhao, D. Laboratory Investigation into Factors Affecting Performance of Capillary Barrier System in Unsaturated Soil. *Water Air Soil Pollut.* **2010**, *206*, 295–306. [CrossRef]
25. Yang, H.; Rahardjo, H.; Leong, E.C.; Fredlund, D.G. A study of infiltration on three sand capillary barriers. *Can. Geotech. J.* **2004**, *41*, 629–643. [CrossRef]
26. Steenhuis, T.S.; Parlange, J.Y. Comment on "The Diversion Capacity of Capillary Barriers" by Benjamin Ross. *Water Resour. Res.* **1991**, *27*, 2155–2156. [CrossRef]
27. Ross, B. The Diversion Capacity of Capillary Barriers. *Water Resour. Res.* **1990**, *26*, 2625–2629. [CrossRef]
28. Hakonson, T.E.; Maines, K.L.; Warren, R.W.; Bostick, K.V.; Trujillo, G.; Kent, J.S.; Lane, L.J. *Hydrologic Evaluation of Four Landfill Cover Designs at Hill Air Force Base, Utah. LAUR-93-4469*; Los Alamos National Laboratory: Los Alamos, NM, USA, 1994.
29. Yunusa, G.H.; Kassim, A.; Gofar, N. Effect of Fine-Grained Soil Layer Thickness on Performance of Modified Capillary Barrier System. *Malays. J. Civ. Eng.* **2015**, *27*, 24–46.
30. Yunusa, G.H.; Kassim, A.; Umar, M.; Talib, Z.A.; Abdulfatah, A.Y. Laboratory Investigation of Suction Distribution in a Modified Capillary Barrier System. In *IOP Conference Series: Earth and Environmental Science*; IOP Publishing: Bristol, UK, 2020; Volume 476. [CrossRef]
31. Ho, C.K.; Webb, S.W. Capillary barrier performance in heterogeneous porous media. *Water Resour. Res.* **1998**, *34*, 603–609. [CrossRef]
32. Harnas, F.R.; Rahardjo, H.; Leong, E.C.; Wang, J.Y. Experimental study on dual capillary barrier using recycled asphalt pavement materials. *Can. Geotech. J.* **2014**, *51*, 1165–1177. [CrossRef]
33. Zhan, T.L.T.; Li, H.; Jia, G.W.; Chen, Y.M.; Fredlund, D.G. Physical and numerical study of lateral diversion by three-layer inclined capillary barrier covers under humid climatic conditions. *Can. Geotech. J.* **2014**, *51*, 1438–1448. [CrossRef]
34. Wu, Y.; Zhou, X.; Liu, J. Long-Term Performance of the Water Infiltration and Stability of Fill Side Slope against Wetting in Expressways. *Appl. Sci.* **2022**, *12*, 5809. [CrossRef]
35. Li, X.; Li, X.; Wu, Y.; Gao, L. A novel unsaturated drainage layer in capillary barrier cover for slope protection. *Bull. Eng. Geol. Environ.* **2023**, *82*, 108. [CrossRef]
36. Kesgin, E. *Investigation of Effective Drainage Methods in Sports Field Under Various Rainfall Conditions*; Yildiz Technical University: Istanbul, Turkey, 2021.

37. van Genuchten, M.T. A Closed-form Equation for Predicting the Hydraulic Conductivity of Unsaturated Soils. *Soil Sci. Soc. Am. J.* **1980**, *44*, 892–898. [CrossRef]
38. Indrawan, I.G.B.; Rahardjo, H.; Leong, E.C. Drying and wetting characteristics of a two layer soil column. *Can. Geotech. J.* **2007**, *44*, 20–32. [CrossRef]
39. Zhang, Y.; Zhang, Z.; Ma, Z.; Chen, J.; Akbar, J.; Zhang, S.; Che, C.; Zhang, M.; Cerdà, A. A review of preferential water flow in soil science. *Can. J. Soil Sci.* **2018**, *98*, 604–618. [CrossRef]
40. Zhang, Y.; Zhang, M.; Niu, J.; Zheng, H. The preferential flow of soil: A widespread phenomenon in pedological perspectives. *Eurasian Soil Sci.* **2016**, *49*, 661–672. [CrossRef]
41. Beven, K.; Germann, P. Macropores and water flow in soils revisited. *Water Resour. Res.* **2013**, *49*, 3071–3092. [CrossRef]
42. Baker, R.S.; Hillel, D. Laboratory tests of a theory of fingering during infiltration into layered soils. *Soil Sci. Soc. Am. J.* **1990**, *54*, 20–30. [CrossRef]
43. Miyazaki, T.; Hasegawa, S.; Kasubuchi, T. *Water Flow in Soils*; Marcel Dekker AG: New York, NY, USA, 1993.
44. Walter, M.T.; Kim, J.-S.; Steenhuis, T.S.; Parlange, J.-Y.; Heilig, A.; Braddock, R.D.; Selker, J.S.; Boll, J. Funneled flow mechanisms in a sloping layered soil: Laboratory investigation. *Water Resour. Res.* **2000**, *36*, 841–849. [CrossRef]
45. Zhang, W.; Sun, C.; Qiu, Q. Characterizing of a capillary barrier evapotranspirative cover under high precipitation conditions. *Environ. Earth Sci.* **2016**, *75*, 1–11. [CrossRef]
46. Barbour, S.L.; Krahn, J. Numerical modelling—Prediction or process? *Geotech. News* **2004**, *22*, 44–52.
47. Bashir, R.; Sharma, J.; Stefaniak, H. Effect of hysteresis of soil-water characteristic curves on infiltration under different climatic conditions. *Can. Geotech. J.* **2016**, *53*, 273–284. [CrossRef]
48. Yang, C.; Sheng, D.; Carter, J.P. Effect of hydraulic hysteresis on seepage analysis for unsaturated soils. *Comput. Geotech.* **2012**, *41*, 36–56. [CrossRef]
49. Likos, W.J.; Lu, N.; Godt, J.W. Hysteresis and Uncertainty in Soil Water-Retention Curve Parameters. *J. Geotech. Geoenviron. Eng.* **2014**, *140*, 04013050. [CrossRef]
50. Wu, L.Z.; Huang, R.Q.; Xu, Q. Incorporating Hysteresis in One-dimensional Seepage Modeling in Unsaturated Soils. *KSCE J. Civ. Eng.* **2012**, *16*, 69–77. [CrossRef]
51. Aubertin, M.; Cifuentes, E.; Apithy, S.A.; Bussière, B.; Molson, J.; Chapuis, R.P. Analyses of water diversion along inclined covers with capillary barrier effects. *Can. Geotech. J.* **2009**, *46*, 1146–1164. [CrossRef]
52. Zhang, L.M.; Ke, Y.Q. Combinations of soil materials for granular capillary barriers for minimizing rainfall infiltration and gas emission. *Can. Geotech. J.* **2017**, *54*, 1580–1591. [CrossRef]
53. Fredlund, D.G.; Rahardjo, H.; Fredlund, M.D. *Unsaturated Soil Mechanics in Engineering Practice*; John Wiley & Sons, Inc.: Hoboken, NJ, USA, 2012; p. 375.
54. Mualem, Y. A New Model for Predicting the Hydraulic Conductivity of Unsaturated Porous Media. *Water Resour. Res.* **1976**, *12*, 513–521. [CrossRef]